Chapter 6

Individual Pulses in Millisecond Pulsars

6.1 Summary

Studies of single pulses from two millisecond pulsars ares presented. The energy distribution of PSR B1534+12 is similar to that of slow pulsars, but extends to somewhat higher energies. There is correlation in the pulse energy on time scales of a few pulse periods. The individual pulses are narrower than the average, but there is no evidence for microstructure which scales with pulse period. The energy distribution of PSR B1937+21 indicates that this pulsar possesses a small number of very strong pulses which are reminiscent of the giant pulses seen in the Crab Pulsar. These large pulses occur in both the pulse and interpulse, and are always delayed relative to the average pulse profile, suggesting that they come from a different emission region, and perhaps are due to a somewhat different emission mechanism. The pulses are delayed about 50μs while the interpulses are delayed about 65μs. No pulse to pulse or pulse-interpulse energy correlations were found, indicating that the phenomenon occurs on extremely short time scales. The delay of these pulses to a location relative to the average profile where the emission is significantly less than the peak average emission implies that they have energies hundreds of times that of the average emission in that region. Pulses or interpulses with total energies > 15 times the mean pulse energy occur about 10 times each in this sample of $757,876$ pulses. Thus these pulses are significantly weaker and occur less frequently than the giant pulses seen in the Crab pulsar. They are energetically unimportant, relative to the average. The average pulse profile of these strong pulses is consistent with the exponential impulse response of the interstellar medium, coupled with some phase jitter between strong pulses. The $\sim 50\mu$s delay between strong pulses and the average suggests a difference in the emission location, corresponding to 7.5 km in altitude, or 11° in phase.

6.2 Introduction

PSR B1937+21, with a spin period of 1.56 ms, was the first millisecond pulsar to be discovered (Backer *et al.* 1982). This relatively new class of pulsars consists of objects with short (millisecond) spin periods, extremely small period derivatives, and therefore weak magnetic fields ($\sim 10^8 - 10^9$ Gauss). The radio emission mechanism of these pulsars, as for normal (slow) pulsars, is not well understood. Due to their weaker magnetic fields, and much shorter spin periods, they may provide new clues to the physics of pulsar emission. In any case, the emission mechanism itself cannot be sensitive to either spin period or magnetic field strength.

The unusually sharp pulse components of PSR B1937+21 have already been noted in Chapter 1. These highlight the difficulty of extending our understanding of slow pulsar geometries to these short spin periods.

Studies of the individual pulses from slow pulsars revealed that the emission is quite erratic, especially when compared to the stable average pulse profiles exploited for precise pulsar timing. The pulse to pulse emission is highly modulated, with fluctuating energies, and varying shapes. Subpulses, micropulses, and their behaviour have been discussed in Chapter 1. There are two possibilities for the origin of the micropulses which are seen in slow pulsars. They could be due either to time variation of the emission beam or to an angular effect. If the emission mechanism does not depend on period, then in the first case structure would be seen on the same time scale in pulsars of all periods. An angular effect would scale with period and be seen on much smaller time scales in millisecond pulsars. The rotation periods of millisecond pulsars are three orders of magnitude smaller than those typical of the slow pulsars. A study of the statistics of the individual pulses of millisecond pulsars allows comparison of the time and angle scales of the emission in the two classes of objects. In addition, a single pulse study of millisecond pulsars may give information about the emission region or mechanism, and how it relates to that in slow pulsars.

The distributions of individual pulse energies for most normal pulsars have maxima somewhat below the mean pulse energy, and are skewed, extending to 4 to 10 times the mean (Hesse & Wielebinski 1974, Backer 1971). The giant pulses of the Crab pulsar discussed in Chapter 5 are exceptional, and have been observed for many years (Heiles, Campbell & Rankin 1970, Staelin & Sutton 1970). Phinney & Taylor (1977) placed strong limits on the existence of giant pulses from other pulsars, using data from Hulse & Taylor (1975). In this chapter, single pulse observations are presented for two millisecond pulsars: PSRs B1534+12 and B1937+21. The pulse-to-pulse energy distribution is analyzed for PSR B1534+12. Observations of giant pulses in PSR B1937+21, are discussed in detail. These were first displayed at 430 MHz and

1400 MHz by Wolszczan *et al.* (1984), while Sallmen & Backer (1995) and Backer (1995) have highlighted their peculiar properties. A separate analysis of the giant pulses from this pulsar has been carried out by Cognard *et al.* (1996).

6.3 Observations & Data Reduction

The data discussed in this chapter were taken at Arecibo on 1992 November 19-22. Signals from the two circular polarizations at 430 MHz were passed through 500 kHz (B1534+12) or 250 kHz (B1937+21) filters and split into real and imaginary parts. This dual polarization complex voltage data was recorded with 2-bit sampling at 1 or 2 μs respectively, or twice the Nyquist frequency. Observing using the ADAGIO package allowed us to record the data with a constant number of samples per apparent period throughout. For PSR B1534+12, which has a period of 37.9 milliseconds, we recorded $\sim$4.1 milliseconds of data for each pulse period, in a window centered on the pulsed portion of the profile. Limited by the speed with which we could write to tape, we were able to record data for 10 out of every 12 pulse periods of PSR B1937+21. These data were coherently dedispersed offline in the frequency domain, using the method described by Hankins & Rickett (1975). The length of the Fourier Transform which is involved was set by the need to include a full dispersed pulse in each transform, resulting in a loss of 3 of the 10 pulse periods for PSR B1937+21. Detection then resulted in dedispersed profiles for 7 out of every 12 pulse periods for this pulsar, and every pulse for PSR B1534+12.

For each of these pulse profiles, the cumulative intensity in windows ON and OFF the pulse were calculated and saved. A $COMPARISON$ window of the same size was located off the pulse, and a larger OFF window was also located away from the pulse. The comparison window was used to estimate the noise distribution for each pulsar, and hence the error in our determination of the energy distribution.

For PSR B1937+21, two windows were designated for both the pulse and interpulse, during the early and late halves of the emission. Two $COMPARISON$ windows of the same size were also used. Initially, only one window was used for each of the pulse, interpulse, and comparison regions, whose widths of 60 (2μs) bins were chosen to contain a large fraction of the emission in the pulse and interpulse. The presence of very strong pulses late in the pulse, where the average emission is low, caused us to increase the size of the windows to 120 bins, to include essentially all of the emission. These larger windows were each split into two 60 bin windows to investigate the possibility that we were selecting against a significant number of narrow late pulses by using only one wide window. At the same time as the energy

calculation, the pulse profile was saved for any pulse in which the average energy per bin in any ON window exceeded that in the OFF window by a given threshold.

$$\frac{E_{window}}{N_{window}} - \frac{E_{Off}}{N_{Off}} > \sqrt{2}T$$

The threshold T used was 5-6 times the estimated error in the mean for 1 pulse, $\overline{E}$. The windows and thresholds used above were determined using an average profile created using a limited amount of data.

6.4 Analysis of PSR B1534+12

The above procedure resulted in an energy *vs.* time series for each of the ON, OFF, and $COMPARISON$ windows, for a given observation. The analysis presented for this pulsar was performed for areas of data for which the effects of interstellar scintillation were judged to be approximately constant.

Figure 6.1 displays the energy histogram obtained for PSR B1534+12 using 12000 pulses. The dotted line shows the distribution of energies in the comparison region (which is centered on zero energy, as expected), while the solid line displays that for the pulse energies. The vertical line indicates the location of the average pulse energy. This distribution has a shape similar to that for some slow pulsars, such as PSR B0950+08 (Backer 1971). However it extends out to about 15 times the average pulse energy, which is not typically found in slow pulsars.

The correlation function for the pulse energies drops to zero for a separation of three pulses, and indicates that there is about 25% correlation between adjacent pulses. The time scale of fluctuations is therefore longer than a pulse period, in contrast to the observations of giant pulses presented here and in Chapter 5. There are no periodicities in the power spectrum of these energies.

The average of the autocorrelation functions for a subset of strong individual pulses was calculated and compared to the autocorrelation function of the average pulse. The results are shown in the first panel of Figure 6.2. The effects of the off-pulse distribution have been removed from the two ACFs, and they have been normalized to the same value at lag 1. These indicate that the individual pulses (dotted line) are somewhat narrower than the average, with a characteristic width of 160 μs *vs* 250 μs. There is no evidence for a break in the ACF on very short time scales and so no evidence for microstructure scaled by the pulse period. There may be evidence for a break at $\sim$ 300 μs, which is not that different from the time scales of microstructure in slow pulsars. Even if there is no break, the characteristic width of 160 μs is also of about this scale. The second panel displays the ACF of the individual pulses, at

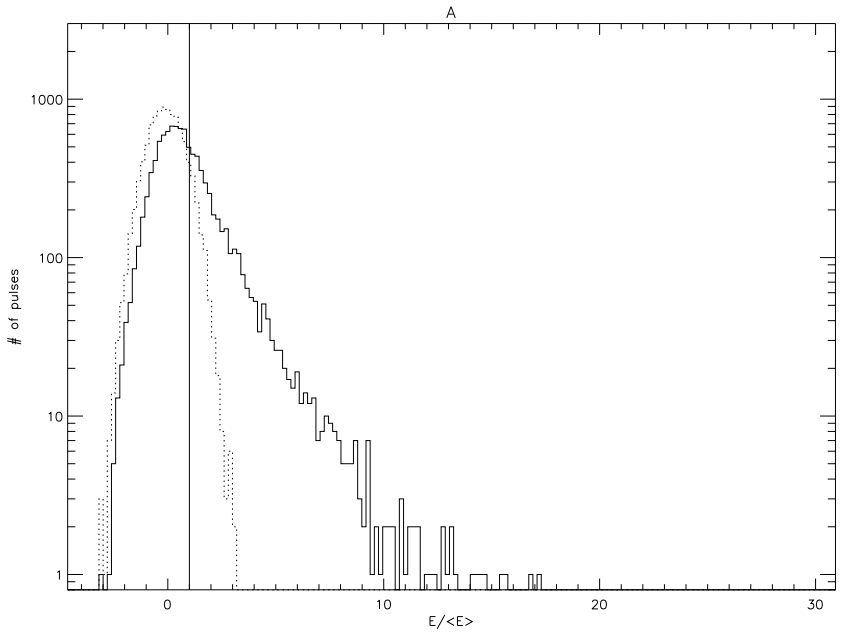

Fig. 6.1.— Pulse energy distribution for PSR B1534+12. The number of pulses for a given energy E are plotted against the pulse energy. The energy axis is in units of the mean pulse energy, $< E >= 7.6$ mJy. The dotted line shows the distribution of comparison energies, while the solid line displays the distribution for the pulsed emission. The solid vertical line represents the mean pulse energy.

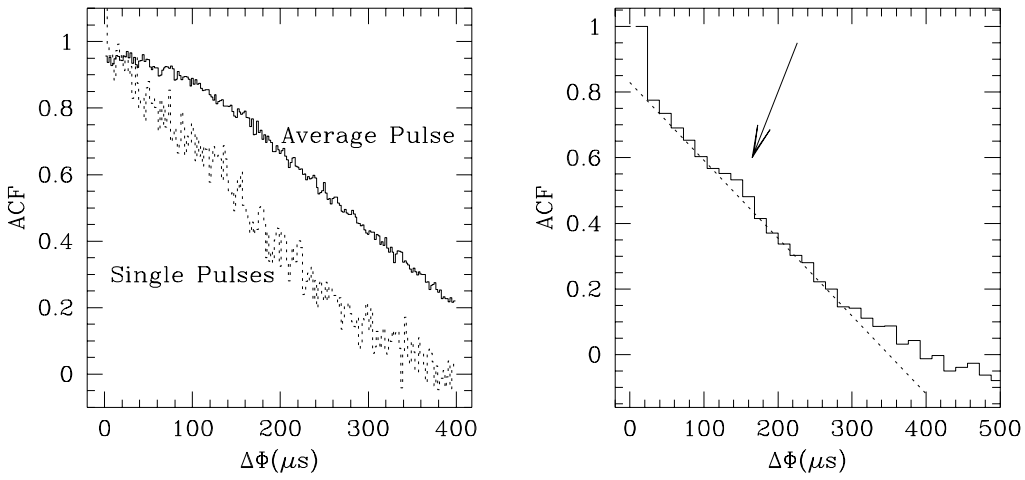

Fig. 6.2.— ACF of individual pulses from PSR B1534+12. The autocorrelation function is displayed for both the individual pulses (dotted line) and the average pulse (solid line) in the first panel. The individual pulses are narrower than the average, but no features are seen on short time scales to indicate that microstructure scales with pulse period. The second panel displays the ACF of the individual pulses at lower resolution, and exhibits a feature at $\sim 150\mu$s.

lower resolution. There is some evidence for an excess at about 150 μs, indicating a possible characteristic time for the emission.

6.5 Analysis of PSR B1937+21

The two windows for the pulse, interpulse, and comparison ranges were combined to produce one energy *vs.* time series for each. These raw time series, $E^R_{[P,IP,C]}(t)$, contain gaps, since we only have profiles for 7 out of 12 periods. The raw series for the OFF window was smoothed, and this baseline level was removed from the series for the other windows, after normalization to energy per bin.

$$E_{[P,IP,C]}(t) = \frac{E^R_{[P,IP,C]}(t)}{N_P} - \frac{< E^R_{Off}(t) >_{\Delta t}}{N_{Off}}$$

The off energy series was smoothed over 4001 data points in the series, corresponding to a time Δt of about 10 seconds. This procedure allows removal of the off-pulse level which slowly varies due to the changing zenith angle of the source during the observation. In addition, an interstellar gain factor was calculated by smoothing the series for the pulse plus interpulse over a similar time scale, $G_{ISS} = a/\overline{a}$ with $a =< E_P(t) + E_{IP}(t) >_{\Delta t}$. This was used to eliminate the slow variations present in the data and expected to be due to interstellar scintillation.

We now consider four observations, taken on four separate days, containing a total of the 757,876 pulses. For each of these observations, the corrected energies, $E^C_{[P,IP,C]} = E_{[P,IP,C]}/G_{ISS}$ were used to determine the mean and rms (distribution width) for each energy series, in addition to the modulation index. The *rms* of the comparison distribution relative to the mean main pulse energy, $\sigma_c/\overline{E}_P$ ranges from 1.1 to 1.4. This means that the signal to noise of the observations is generally low, but somewhat variable. The average interpulse energy is $\overline{E}_{IP} = 0.6\overline{E}_P$ in all cases.

The modulation index $m_{P,IP}$ of a series pulse or interpulse energies $E_{[P,IP]}(t)$ is given by equation 1.1, and reflects the variability in the time series. In slow pulsars, those which have high modulation indices typically have energy distributions which extend to higher energies than those with smaller modulation indices. For the observations discussed here, $m_P \sim .51 - .55$, $m_{IP} \sim .59 - .65$. Thus the interpulse emission is more modulated than that from the main pulse, and the overall level of modulation is less than 100 %. If the early and late halves of the emission are treated individually, we find $m_{P_1} \sim .57 - .59$, $m_{P_2} \sim 1 - 1.5$, $m_{IP_1} \sim .67 - .73$, and $m_{IP_2} \sim 1.4 - 1.5$. Thus more of the fluctuations take place in the late half of the pulse emission.

The corrected energies were used to create a histogram of number *vs.* energy for each observation. Figure 6.3 displays the energy histogram for 757,876 pulses of

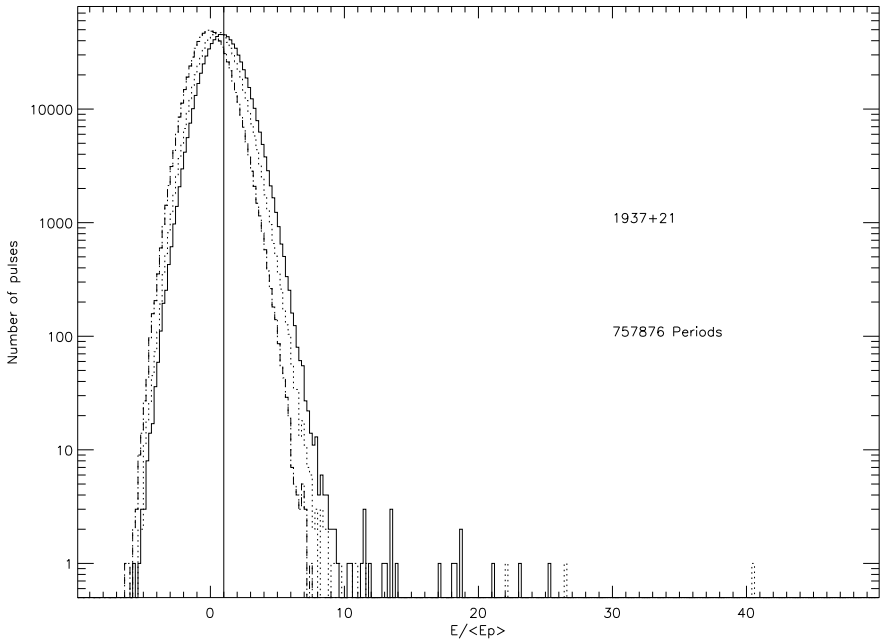

Fig. 6.3.— Probability density distribution of pulse energies. The Number of pulses *vs.* Pulse energy is displayed for 757 876 pulses of data for PSR B1937+21. The energy axis is in units of the average energy in the main pulse. The dashed line shows the distribution of comparison energies, indicating the distribution of noise. The main pulse and interpulse distributions are indicated by the solid and dotted lines, respectively.

data for PSR B1937+21, which includes information from four separate observations. The energy axis is in units of the average energy in the main pulse. This allows the intensity variations from day to day due to ISS to be removed. They will, however, have an effect on the width of the comparison distributions for the four observations relative to this energy scale. In addition, the number of 6 sigma pulses will vary for the four observations, at least in part because the cutoff is different in terms of the mean energy. The dashed line shows the distribution of energies in the comparison region (which is centered on zero energy, as expected by construction, since $E_C \sim E_{Off}$), while the solid and dotted lines display the energy distributions of the main pulse and interpulse respectively. The width of the comparison distribution is an indication of the noise present in our energy determinations.

It is clear that the SNR is poor, in that the average main pulse energy is significantly less than the width of the comparison distribution. This implies that a typical single pulse cannot be observed. The energy distribution for the pulse and interpulse emission is, however, broader than the comparison distribution, and is shifted from zero, due to the presence of pulsed emission. This portion of the distribution extends

to energies about 10 times the average pulse energy. There are, however, several main pulses and interpulses which are much stronger than the typical ones. Individual pulses of this strength are seen only here and in the Crab pulsar. Note that the energy scale is in units of $\overline{E}_P$. This means that the strong interpulses are stronger by a factor of 1.67 relative to the average interpulse energy $\overline{E}_{IP}$. There are 23 main pulses and 12 interpulses with energies more than 6 sigma above the mean energy for their respective observations (after correction for interstellar scintillation). Of these, 21 main pulses and 10 interpulses met the threshold for output during processing, and so were extracted and examined. One each of these strong pulses and interpulses are displayed in Figure 6.4, along with the average for the observation which included the strong pulse. The vertical lines on the average profile indicate the limits of the windows used to analyze the energies. Strikingly, the strong pulses are always located at the trailing edge of the average pulse components. Thus we found it necessary to ensure that this region was included in the windows used to calculate the energies, although little of the average pulse energy is contained in this region.

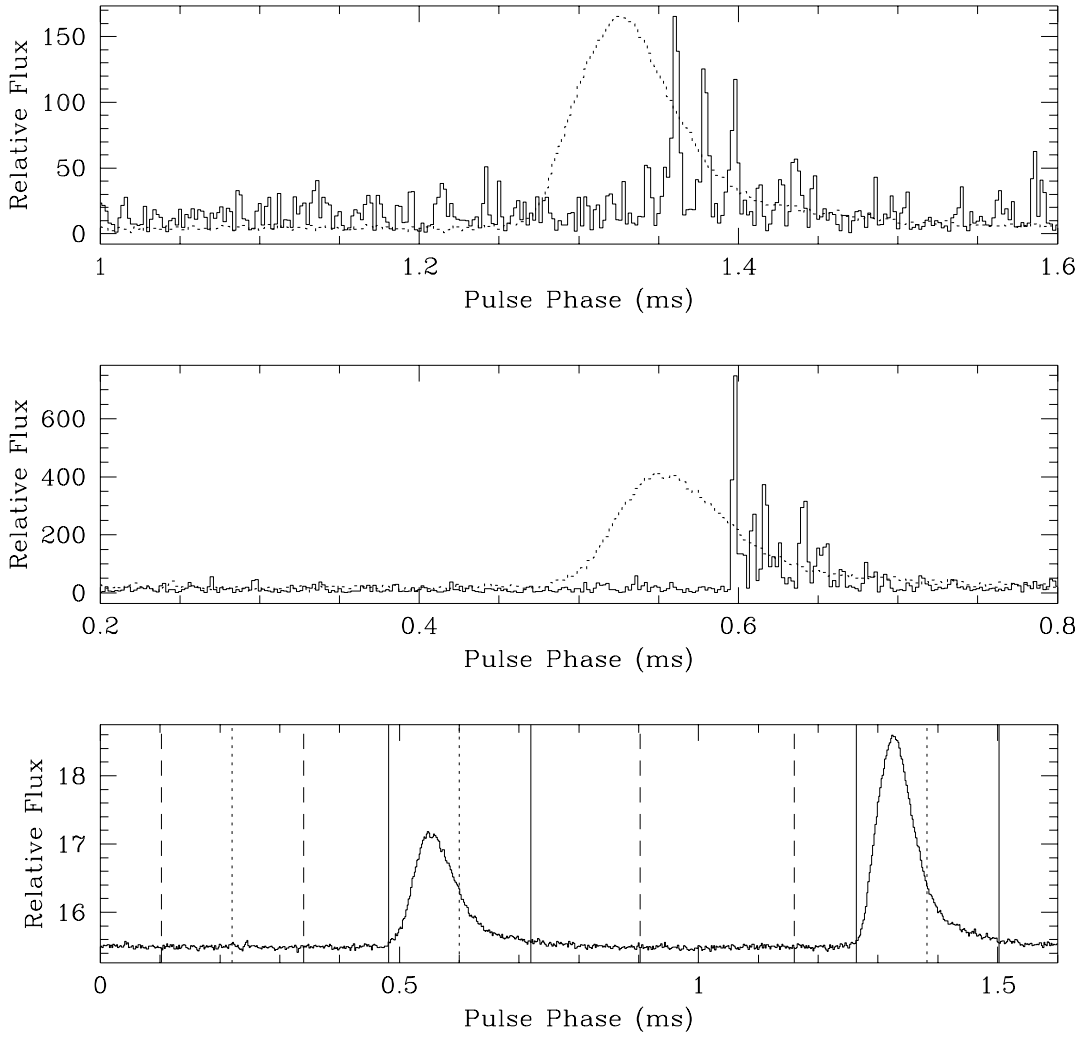

Fig. 6.4.— Very strong main pulse and interpulse from PSR B1937+21. The bottom panel displays the average pulse profile, containing 196 868 pulses. The solid vertical lines indicate the boundaries of the *ON* windows in the pulse and interpulse regions. The dashed vertical lines indicate the boundaries of the comparison region and the region used to determine values off the pulse. The dotted vertical lines indicate the separation of the pulse, interpulse, and comparison windows into two halves, as discussed in the text. The top panel shows one of the very strong pulses, while the middle panel displays a very strong interpulse. The Relative Flux scale is the same for the three panels. In each of the top two panels, the dotted line shows the location of the average pulse profile relative to the individual pulses, although here the average profile is no longer on the same flux density scale.

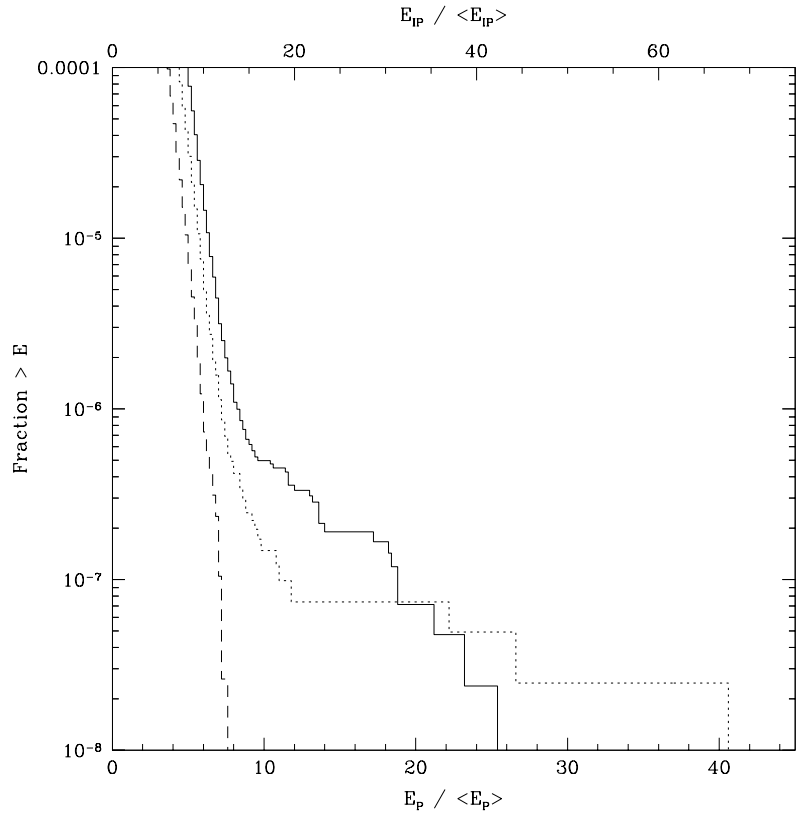

Fig. 6.5.— Integrated probability density distribution for Very strong pulses. The cumulative Number of Pulses *vs.* Energy is displayed for 757 876 pulses of data. The bottom axis is in units of the average main pulse energy, while the top axis is in units of the average interpulse energy. Solid, dotted, and dashed lines display the main pulse, interpulse, and comparison distributions.

6.5.1 Giant Pulses

The strong pulses, like the average profile, are broadened by interstellar scattering. The impulse response of the interstellar medium (ISM) is given by the one-sided exponential in equation 1.19, for a simple single thin screen model of scattering. The presence of the strong pulses only in this exponential scattering tail due to the interstellar medium raises the possibility that they are not intrinsic to the pulsar, but due to some propagation mechanism in the ISM. But this cannot be the case. There is no pulse to pulse energy correlation at the 1 percent level, and no correlation between main pulse and preceding or following interpulse energies at the 2 percent level. Inspection of the strong pulses also revealed that the giant main and interpulses occur independently. This means that the effect has a time scale of less than one pulse period, or approximately 1.6 ms, which is much shorter than any time scale on which the ISM is expected to vary. The time scale for the diffraction pattern to change is many seconds at 430 MHz, for example (Cordes *et al.* 1990).

Figure 6.5 displays the cumulative fraction of pulses with energy $E < \overline{E}$. The scale on the bottom axis is in terms of $\overline{E}_P$, while that on the top axis is in terms of $\overline{E}_{IP}$. There are 46 main pulses which occur with energy $E_P > 8\overline{E}_P$, 21 with $E_P > 10\overline{E}_P$, and 13 with $E_P > 13\overline{E}_P$. There are no main pulses with energies $E_P > 26\overline{E}_P$. In the interpulse distribution, on the other hand, there are 3 interpulses with energies $E_{IP} > 30\overline{E}_{IP}$. There are 20 interpulses with energies $E_{IP} > 13\overline{E}_{IP}$. The interpulse distribution becomes significantly contaminated by the comparison distribution below this point. It seems, however, that more strong interpulses occur at this level than do strong pulses, and that the interpulse distribution extends to higher energies. The fact that $m_{IP} > m_P$ is consistent with this picture. If much of the modulation is due to these strong pulses or interpulses, the larger modulation index for interpulses implies either that there are more large interpulses, or that they occur with larger energies, or both. This behaviour is not confirmed by the larger data set of Cognard *et al.* (1996, who find that the fractional rate of occurrences are the same for both the main pulse and the interpulse.

The strong pulses shown in Figure 6.4 occur tens of microseconds later than the peak of the average pulse emission. This behavior is consistent in all the strong pulses studied. Because the strong pulses occur only in the exponential scattering tail of the average profile, they are actually much stronger relative to the average energy in that portion of the profile than is apparent in the energy scale of Figure 6.3. This makes their energies hundreds of times that of the average. This is shown in Figure 6.4, as all profiles are on the same relative flux scale.

Since these giant pulses only occur late relative to the average emission, they should produce extra modulation in the second half of the emission. This is consistent with the 100 % modulation for this portion of the emission region which was found earlier. These pulses evidently cause a significant fraction of the energy modulation for this window.

The phase of the 21 and 10 very strong main pulses and interpulses relative to the arrival of the average pulse was determined by cross correlating their profiles with the appropriate average profile. The strong pulses associated with the main pulse occur with a delay of $48 \pm 4.4\mu$s, while the strong interpulses occur with a delay of $66 \pm 4.6\mu$s. Both these delay values are larger than those quoted by Cognard *et al.* (1996), although the difference is $> 3\sigma$ only for the interpulse. Inspection of Figure 2 of Wolszczan *et al.* (1984) indicates that at 1384 MHz the strongest main pulses appear to arrive latest, with the strongest displayed pulse offset $45 - 50\mu$s from the average. It is intriguing that the delays between the average profile and the strong main pulses correspond to the location of the small secondary maxima in the average 1410-MHz main pulse and interpulse profile displayed in Figure 3.25. These

secondary maxima are also visible as shoulders in the 800-MHz profile displayed in that figure. Any such features in the average 575-MHz profile are hidden by the exponential scattering tail.

The averages of the very large main pulses (21) and interpulses (10) were generated. This was done by determining the relative phases of the averages for the four observations by cross-correlation. The individual pulses from the four observations were then shifted relative to each other by these same amounts, and then averaged. No attempt was made to further align the individual pulses. Several attempts were made to fit these average profiles by simple functions. The impulse response of the interstellar medium discussed earlier suggests use of a one-sided exponential, $exp(-t/t_{exp})$. A fit made by requiring the area of the pulse (or interpulse) average to equal the area of this exponential, and requiring the same decay time for both (since they pass through the same ISM) is shown in the top panel of Figure 6.6. This simple model works remarkably well. The interstellar broadening time $t_{exp} \sim 52\mu$s found here is somewhat longer than $\sim 30\mu$s time scale for broadening τ_B expected for this pulsar (Cordes *et al.* 1990). This simple model cannot, however, account for emission on the leading edge of the average. Such emission must be due either to the fact that the ISM is not a thin screen, or that the intrinsic average pulsar emission for these pulses is not an impulse. A simple addition to the thin screen model involves two thin screens. The appropriate fitting function is then the convolution of two exponentials, and is of the form $exp(-t/t_2)[1-exp(-t/t_1)]$. (unless $t_1 = t_2$, then the form is $t\ exp(-t/t_1)$). This model of the ISM yields the fit shown in Figure 6.6, with $t_1 \sim 14\mu$s and $t_2 \sim 36\mu$s. This does a better job of matching the emission on the leading edge, and drops to $1/e$ of its maximum value approximately 47μs past the peak. Fitting using a smoothed one-sided exponential approximates the effect of individual pulses having exponential shapes (each one being intrinsically an impulse), but with some dither in phase from pulse to pulse. Individual pulse studies of slow pulsars have revealed that the phases of individual pulses do vary within the pulse window, indicating that this is a reasonable model. A reasonable fit here is obtained with $t_{exp} \sim 42\mu$s, and rectangular smoothing lengths of 30μs and 18μs for main pulse and interpulse, respectively. Once again, the leading edge emission is accounted for, as can be seen in Figure 6.6. The value of t_{exp} found for this model is closest to the expected $\tau_B \sim 30\mu$s. These last two models are better fits to the data than the simple exponential, and produce similar reduced chi squared values. These values are not one, because the average profiles are quite noisy. The portion of the chi squared value associated with the interpulse average is significantly larger, which is not surprising given that it appears noisier. These averages are noisy because they contain a small number of strong pulses, each of which contains sharp structure on short time scales. In contrast to these results,

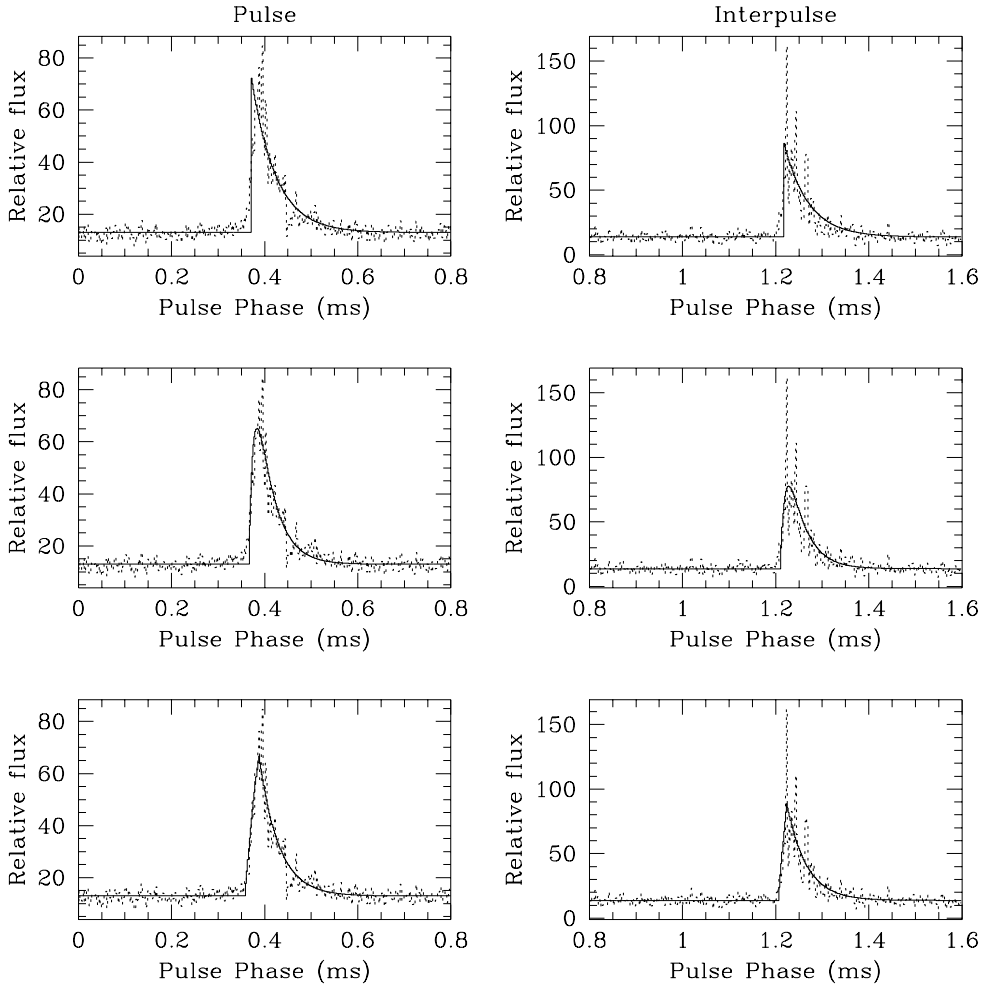

Fig. 6.6.— Shape of very strong pulses in PSR B1937+21. The dashed lines for all panels on the left hand side display the average profile for 21 very strong main pulses. The dashed lines for all panels on the right hand side display the average profile for 10 very strong interpulses. The solid lines in the top two panels are for the best fitting model of the form $e^{-\frac{t}{t_{exp}}}$. In the middle two panels, the solid lines are for the best fitting model for the convolution of two exponentials, while the bottom two panels contain the model for exponentials with smoothing.

Cognard *et al.* (1996) found no evidence for jitter in giant pulse arrival times; their giant pulse average has a rise time of 5 μs, and their exponential decay time of 25μs is comparable to the expected value. More giant pulses were included in their averages, which may account for some of the discrepancy.

6.5.2 Temporal variations

The very strong pulses discussed above show extremely sharp features. From the impulse response of the ISM we expect an exponential envelope, plus noise with the number of degrees of freedom related to the time-bandwidth product, $\sqrt{Bt}$, here

corresponding to intensity modulations of 71%. This is in general agreement with the observations. Emission intrinsic to the pulsar could be even stronger, and as sharp as a microsecond. If this were true, it would argue that microstructure scales with period, and is thus largely an angular effect. Alternatively, most of the structure shown could be due to amplified system noise.

A reasonable model of pulsed emission is the amplitude modulated noise (AMN) model of Rickett (1975). In this model, the pulsar field $g(t)$ is given by $g(t) = a(t)n(t)$, where $a(t)$ is a real amplitude modulation, containing any subpulse or micropulse time variations, and $n(t)$ is an uncorrelated noise process. Then the intensity $I(t)$ is given by $I(t) = [\eta T_{sys} + |g(t)|^2]$, and contains the fluctuations of $a(t)^2$. But the error ΔI in our estimation of $I(t)$ is proportional to $I(t) = [\eta T_{sys} + |g(t)|^2]$, which contains a contribution due to the source (pulsar). When $a(t)$ is large, *ie* the pulsar is extremely strong, ΔI is also large. So for extremely strong pulses, sharp fluctuations may be due either to system noise amplified by the source, or to intrinsic fluctuations of the pulsar.

The main pulse shown in Figure 6.4 contains a remarkable triple feature. It is possible that these are all due to one impulse from the pulsar, separated due to varying propagation paths in the ISM. The exponential envelope expected for the impulse response of the ISM is based on the Gaussian probability of scattering into an angle theta, and is thus true only in a time averaged sense. Instantaneously, individual paths with different scattering delays and amplitudes may be relevant. This would also lead to fluctuations in the pulse profile that don't appear noise-like.

A classic test for microstructure is to calculate the autocorrelation function (ACF) of the pulse profile data. Changes in the slope of the ACF at a given lag $t_\circ$ indicate the existence of significant structure on time scales $\lesssim t_\circ$. Here, however, we don't really have the signal to noise to test for microstructure in this fashion. We must find another way to determine the significance of the sharp fluctuations in our data.

Are the sharp fluctuations in our strong pulses due to real variations in $a(t)$, or are they consistent with amplified system noise? If they are consistent with amplified system noise, then there is some true underlying 'smooth' distribution, with a realization of system noise superimposed upon it. Let $< I(t) >_{\Delta t}$ be a running mean of $I(t)$ calculated over Δt, and $I_n(t, \Delta t) = I(t)/ < I(t) >_{\Delta t}$. Then if $< I(t) >_{\Delta t}$ is the true underlying distribution, and any extra fluctuations are due to system noise, then the probability density function (PDF) of $I_n(t, \Delta t)$ in the region of the pulse will be the same as the PDF of the system noise in a region off the pulse. If Δt is 2μs, however, then $< I(t) >_{\Delta t} = I(t)$, and $I_n(t, \Delta t) = 1$, so its PDF is a delta function, and very unlike the PDF of the off pulse system noise. If Δt is large compared with the time scale of true fluctuations in $a^2(t)$, then the PDF of $I_n(t, \Delta t)$ will contain an

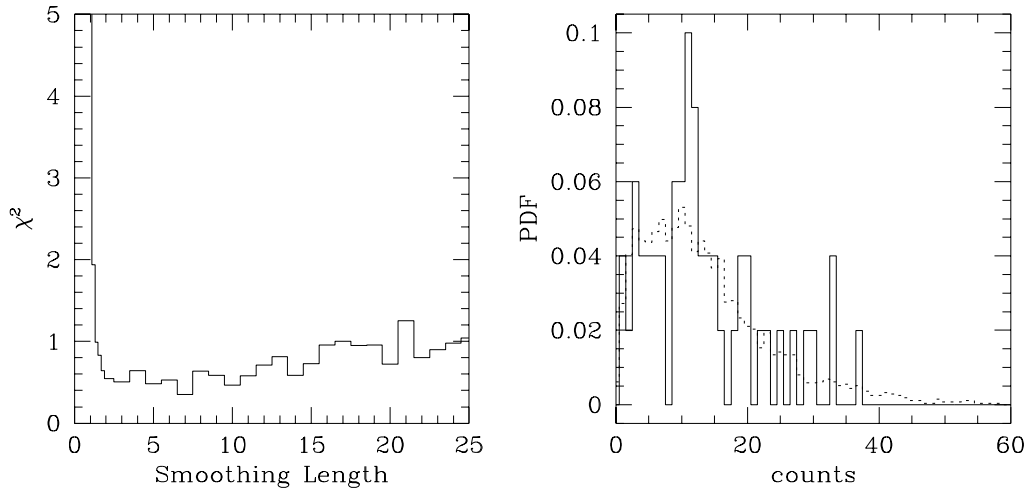

Fig. 6.7.— χ^2 of PDF for a very strong pulse. A running mean of the data for this pulse was calculated over Δt, and this was used to normalize the data at each point. The probability density function of the resulting values in a region centered on the pulse was compared to the corresponding PDF for a region away from the pulsed emission. The first panel displays the χ^2 quantity of this comparison for a variety of smoothing lengths Δt. A distinct minimum for a given Δt would indicate emission with that characteristic time scale. The second panel displays the PDF for the on-pulse region (solid line) and the PDF for the off-pulse region (dotted line) for the smoothing length with the smallest χ^2.

excess at large values relative to that of the off pulse system noise. So comparison (in a χ^2 sense) of the PDF of $I_n(t, \Delta t)$ with the off pulse PDF for a variety of Δt values will produce a minimum in the chi squared distribution at Δt equal to the time scale of fluctuations in $a^2(t)$. This is similar to analysis performed by Bartel and Hankins (1982). They compared the PDF of I_n to the expected exponential distribution e^{-I_n} for noise. Here, we compute the off PDF explicitly.

For several strong pulses and interpulses, the above procedure was performed for a variety of smoothing lengths. A typical example of the results is shown in Figure 6.7. The expected peak in the chi squared distribution at a smoothing length of one bin (2μs) is clear, but there is no well defined minimum. This implies that we are unable to detect any intrinsic variations on these times scales. It is still possible that there are intrinsic variations on time scales shorter than can be resolved.

This result, coupled with the fact that the average of the strong pulses is consistent with the impulse response of the interstellar medium plus phase jitter, indicates that these very strong pulses are extremely sharp; narrower than our 2μs resolution.

6.6 Discussion of Giant Pulses

6.6.1 Comparison to the Crab Giant Pulses

Giant pulses have been found only in this pulsar and the Crab pulsar. Many of their properties are similar, while others are strikingly different. The delayed nature of the giant pulses in PSR B1937+21 is very different from the observed behaviour of the Crab giant pulses. Lundgren (1994) finds no offset between the Crab giant pulses and the average, although Friedman & Boriakoff (1990) find that the giant pulses may occur *earlier* in this object.

The giant pulses in the Crab pulsar are energetically important, as was discussed in Chapter 5, contributing a larger fraction of the total energy at higher frequencies. For the 1937+21 data presented here, the main pulses with energy $E_P > \overline{1}0E_P$ contribute less than 0.05% of the total main pulse energy. This is insignificant, despite the fact that each pulse is very large relative to the average at its phase. The interpulses with energy $E_{IP} > 13\overline{E}_{IP}$ contribute about 0.05% of the total interpulse energy. Thus it seems as though the strong interpulses are slightly more important energetically, but still insignificant at 430 MHz. They may be more important at higher frequencies, however, if they behave as do the giant pulses in the Crab.

Cognard *et al.* (1996) noted that the giant pulses occur at similar rates in the two pulsars. Their data, and Figure 6.3 suggest that the giant pulses may form a separate distribution in this object, just as they do in the Crab pulsar (Lundgren *et al.* 1995). No correlations have been found between adjacent or nearby pulses or interpulses for either pulsar. The time scale of the effect producing the large pulses is extremely short, less than one spin period.

The pulse-interpulse morphology of the average PSR B1937+21 profile is similar to that of the multi-wavelength components in the Crab profile. Any conclusions drawn based on this similarity are highly speculative, especially since these two components of the Crab may be produced in a different location in the magnetosphere than the radio precursor. For either pulsar, attempts at profile classification using the methods successful for normal pulsars encounter difficulties.

6.6.2 Models of the Emission Beam

One of the most striking features of the strong pulses in PSR B1937+21 is that they are delayed relative to the average of the weaker pulses. As noted above, the shape of the pulse profile in the Crab pulsar does not change for the giant pulses. However, shape changes with intensity have been reported for some slow pulsars.

Krishnamohan and Downs (1983) reported shape changes with intensity in the Vela pulsar, in which the stronger pulses arrived progressively earlier. They modelled these shape changes as due to the presence of a number of components which fluctuate independently (and are allowed to drift in position with intensity). They concluded that each component is produced at a different distance from the neutron star, and that these distances may vary with the intensity of the component. This model, combined with the rotating vector model for each component, correctly explains the changes in polarization position angle with pulse intensity. In this view, emission altitude is related to pulse intensity.

McKinnon and Hankins (1993) found shape variations with intensity in PSR 0329+54. Once again, the stronger pulses arrive earlier. For this pulsar, the assumptions of Krishnamohan & Downs (1983) would result in components whose emission altitudes conflicted with that expected from Rankin's (1990) classification of the pulsar, if emission fills the open field line region. Instead, McKinnon and Hankins interpreted the data as an indication of a 'hot' spot on the surface with a varying location. The strong core component is more aligned along the line of sight when it appears earlier in the pulse profile, and so appears more intense. In this model the hot spot moves by less than 43 m, where the diameter of the polar cap is 240 m. Thus correlations between pulse intensity and pulse phase have been explained in two very different ways in the above two cases.

In the case of PSR B1937+21, we have an offset between the large pulses and the average profile, implying a different emission location for the large pulses. The temporal offset could be due either to different altitudes of emission, horizontal separation at a constant altitude, or a combination of the two effects. A temporal offset of 50μs corresponds to a difference in altitude of $c\Delta t/(1+\sin\alpha) \sim 7.5$km $\sim R_{NS}$, about one neutron star radius. The light cylinder for this pulsar is at a distance of only 75 km $\sim 5R_{NS}$. Thus a change in altitude of 7.5 km for the two types of emission is a significant fraction of the distance to the light cylinder. Such a change is altitude would be somewhat surprising since Cordes and Stinebring (1984) used multifrequency measurements to determine that all emission from this pulsar arises from the same altitude to within ± 2 km. The same 50μs offset could be explained by a separation of about 11° in phase. This corresponds to $2-3$ km on the neutron star surface, and is well within the size of the polar cap predicted by the last open field line. If this were the case, then the $\sim 30\mu$s jitter between various large pulses corresponds to ~ 1.5 km motion of this region.

The fact that the giant pulses in the Crab pulsar appear to come from a separate distribution implies that there is a different emission mechanism, or different emission location within the magnetosphere, or possibly both of the above, for the giant and

weaker pulses. However, lack of an offset in the timing residuals between giant pulses and the average pulse profile suggests that the emission region is the same.

The temporal offset of the large pulses in PSR B1937+21 strongly suggests a different emission location for these pulses, as discussed above. If the large pulses come from a different location, they may also be produced via a somewhat different emission mechanism. Their narrowness and temporal offset perhaps point to some sort of maser mechanism.

Due to the temporal separation, these strong pulses cannot simply be due to a temporal modulation of the pulsar beam. It is possible, however, that the very strong pulses are due to a separate narrow component with some temporal modulation. In this case, the emission is clearly in a high state for less than one pulse period. The above analysis of the sharp rise in the giant pulse profile indicated that the width of the large pulses is only a few μs (the width of the interstellar scattering tail makes it difficult to be precise), and perhaps much less. The average size of the beam corresponding to this component is reflected in the arrival time jitter between pulses. The 3σ arrival time variation among these pulses is about 15μs, while the model using pulse jitter and the ISM indicates such variations could be as much as 30μs. If each large pulse is broadened solely due to interstellar propagation, then the high state duration is only a few microseconds, and is smaller than this average beam size. If, on the other hand, the width of the individual large pulses is approximately the same as the jitter between pulses, the high state duration lasts at least as long as this $15 - 30\mu$s, and possibly almost as long as a period.

If these individual pulses are due to an angular modulation, then the measured width of their average corresponds to a beam less than $\sim 20\mu$s wide (as determined from the rise time of the giant pulse average), and possibly much smaller. For giant pulses with beam width $w_{\rm gp}$, occurring a fraction f of the time, the wobble perpendicular to the trajectory of the line of sight (in the ϕ direction) is $w_{\rm gp}/(Pf)$. Then a jitter of 30 μs $\sim 6.75^\circ$ along the observer's line of sight implies that for the same jitter in the ϕ direction, giant pulses would be observed much more frequently than is the case. For a 1 μs beam, about 1 of every 30 pulses is expected to be giant! This cannot be reconciled with the observed low occurrence (of order 1/10000) of giant pulses for a circular beam, unless the beam width is less than 0.003μs. This corresponds to a region with a radius of only 3 cm on the neutron star surface.

Thus the strong pulses in PSR B1937+21 are probably produced in a different region than the average weaker pulses, possibly in a temporally modulated separate component. It is intriguing that similar effects are found in the main pulse and in the interpulse, since these are supposedly two separate poles. On the other hand, the main pulse and interpulse features of the Crab pulsar are believed to originate high in

the magnetosphere, with both components resulting from emission from a single pole (Romani & Yadigaroglu 1995), and some authors believe this model may be extended to other young radio pulsars (Manchester 1996). If the emission does originate from two poles, then the mechanism is stimulated in both places by the properties of the pulsar. It is surprising, however, that such a phenomenon could produce not only strong pulses in both poles, but the similar relative delays. These relative delays are not equal, however, so the two poles need not be identical.

6.6.3 Further Studies

Since the very strong pulses discussed in this paper occur in the scattering tail, data at higher frequencies such as 1400 MHz would make possible better measurements of the individual pulse widths, which would help to constrain the models for the emission of these strong pulses, as well as clarifying the relationship between these very strong pulses and the narrow trailing components visible in the average pulse profile. In addition, if these events are related to the Giant Pulses in the Crab pulsar, they may become energetically more important at higher frequencies, and thus be easier to study. However, inspection of archival data taken in Arecibo showed no evidence for giant pulses at 1400 MHz, at the level of about 30 times the average pulse energy (corresponding to energies ~ 100 times the average energy on the trailing edge of the pulse).

Similar studies of other millisecond pulsars can tell us if these events are isolated to this object, or whether they are common in millisecond pulsars. Some millisecond pulsars have profiles with sharp features similar to that of this pulsar, while others contain emission spreading over much of a pulse period (as would be expected from the width of the last open field lines for these short period objects). Perhaps the presence of these events in PSR 1937+21 is related to the unexpected sharpness of its components. Cognard *et al.* (1996) suggest that the unique properties of the Crab pulsar and PSR B1937+21 may be due to the large strength of the magnetic field at the light cylinder, $B_{LC} \sim 10^6$ Gauss. All other pulsars have weaker B_{LC}. Pulsar B1957+20 has the next strongest B_{LC}, of $\sim 4 \times 10^5$ Gauss. Early analysis of some 430-MHz data on PSR 1957+20 revealed no similar features, although this object is significantly weaker, and strong pulses with energies above 125 times the average energy would be required for such events to appear. Pulsar J0437−4715 is nearby and very strong. Single pulse studies have revealed that the strongest individual pulses are very narrow, and preferentially located within the average profile, resulting in profile variations with intensity (Anderson *et al.* 1996, Ables *et al.* 1997). No truly giant pulses have been seen, nor is there any evidence for microstructure or a preferred time scale for the emission (Jenet *et al.* 1998).

6.7 Conclusions

Single pulse observations of two millisecond pulsars were presented in this chapter. The giant pulses of PSR B1937+21 are similar to those found in the Crab pulsar. They are, however, *delayed* relative to the average pulse profile, and correspond to features on the trailing edges of the components in high frequency average pulse profiles. This suggests that they come from a different emission region, and perhaps are due to a somewhat different emission mechanism. The observations are difficult to explain with a simple randomly wobbling circular beam. It is possible that giant pulses occur due to temporal modulation of a separate component of emission. No pulse to pulse or pulse-interpulse energy correlations were found, indicating that the phenomenon occurs on extremely short time scales. The delay of these pulses to a location relative to the average profile where the emission is significantly less than the peak average emission implies that they have energies hundreds of times that of the average emission in that region, although they are too rare to be energetically important at this frequency. The average pulse profile of these strong pulses is consistent with the exponential impulse response of the interstellar medium, coupled with some phase jitter between strong pulses. No giant pulses were seen in this object at 1400-MHz, and they occur uniquely in PSR B1937+21 and the Crab pulsar. The single pulses presented for PSR B1534+12 are correlated on time scales of a few periods, with no periodicities evident in the power spectrum. The pulse energy histogram extends to slightly higher energies than is typical in slow pulsars, but is otherwise similar. No evidence for microstructure which scales with period are seen.